Hindawi Publishing Corporation
X-Ray Optics and Instrumentation
Volume 2010, Article ID 156984, 9 pages
doi:10.1155/2010/156984

Research Article

Multi-MeV Flash Radiography in Shock Physics Experiments: Specific Assemblages of Monolithic Scintillating Crystals for Use in CCD-Based Imagers

D. Partouche-Sebban, I. Abraham, S. Lauriot, and C. Missault

CEA, DAM, DIF, 91297 Arpajon, France

Correspondence should be addressed to D. Partouche-Sebban, david.partouche@cea.fr

Received 14 October 2010; Accepted 8 December 2010

Academic Editor: F. Patrick Doty

We have developed a new CCD-based radiographic camera called CrystalEyeCam for use in shock physics experiments: it is composed of two turning mirrors and an objective to relay the (visible) image from a scintillator assembly to a highly sensitive, low noise CCD camera. The objective was specifically developed to match our needs and has few chromatic and geometric aberrations and high photometric performance. The scintillator assembly is constructed using a specific (patented) technique of assembling monolithic scintillating crystals. It replaces the segmented scintillator previously used at our facility and produces higher quality images (better resolution and no segmentation). The sensitivity, noise level, detection threshold and resolution of CrystalEyeCam were measured using an 18-MeV-bremsstrahlung spectrum, filtered with 10 cm of lead, and two 165 mm × 165 mm BGO assemblies: 20 and 30 mm in thickness, respectively. In particular, with the 30 mm-thick BGO assembly, the measured detection threshold of the imager (at $SNR_0 = 2$) is 1 μGy(air) and its resolution is ∼1 mm. For 4-MeV incident photons, the estimated (energy) stopping power of the scintillator is 41%. The scintillator assembly thus proved to be a cheaper, effective alternative to segmented scintillators for use in CrystalEyeCam.

1. Introduction

The radiographs produced at the AIRIX facility (induction LINAC for flash radiography and X-ray imaging [1]) provide fundamental experimental data for studying the dynamic behaviour of materials under the effects of chemical-explosive detonation. In shock physics experiments, explosives can impart speeds as high as a few kilometers per second to the studied metal. As a result, in order to minimize the effect of motion blur on the radiographs, the X-ray source pulse duration must be no more than a few tens of nanoseconds, thus limiting the available level of dose. In addition, the studied objects are generally rather thick and made of high-density materials. The harsh experimental environment (i.e., the use of explosives) also requires use of blast protection materials. Consequently, even though AIRIX produces high-energy X-rays (up to ∼19 MeV) and a significant dose level, relatively few photons manage to pass through the object and the blast protection layers. And those that actually reach the imaging system are only the most penetrating X-rays (typically 1 to 6 MeV in energy). As a result, high-stopping-power imagers are needed in such experiments, and the use of high-density scintillating crystals, to convert the X-ray image into visible light, is thus particularly beneficial. Such scintillators can be optically coupled to highly sensitive, low-noise photometric cameras to produce high-performance, linear radiographic imagers.

We have developed a CCD-based radiographic camera called CrystalEyeCam; this system was initially designed to be used with segmented scintillators, but we recently upgraded it to use a specific assemblage of monolithic scintillating crystals to access higher quality images at the facility and, thus, improve the precision on the observations of the phenomena of interest. During its development period, prior to its eventual installation at AIRIX in 2009, the imager was regularly fielded at the ELSA facility [2] in order to

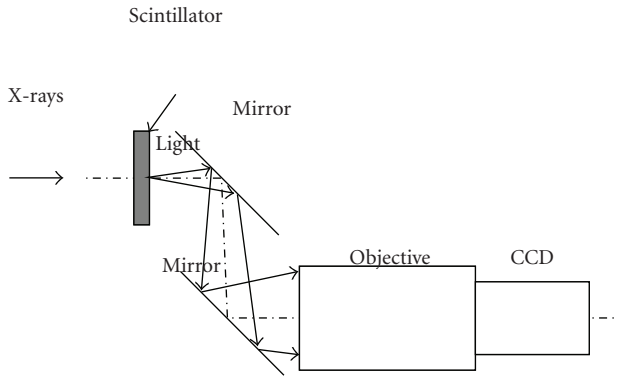

Figure 1: Sketch of CrystalEyeCam radiographic camera; it uses a scintillator to convert X-rays into light, a set of two turning mirrors and an objective to relay the visible image from the scintillator to the CCD. The turning mirrors allow offsetting the CCD and the objective lenses from the direct X-ray flux.

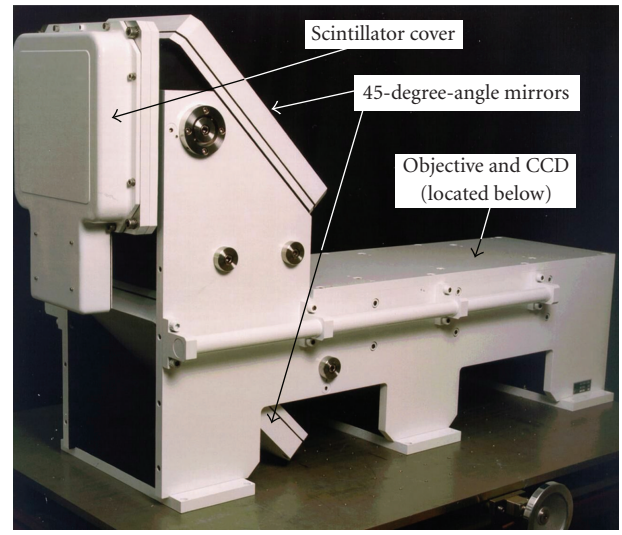

Figure 2: Photograph of the CrystalEyeCam camera. The system is about 140 cm × 50 cm × 80 cm in dimension. The X-ray scintillator is located under the front cover (on the upper left of the image). The first 45-degree-angle mirror is visible in the upper part of the device (on the right edge of the upper cover) and the second one is partially visible below the first one (in the lower part of the device). The objective and CCD camera are cased inside the horizontal section.

evaluate various scintillating assemblies and to measure the imager performance (sensitivity, noise level, detection threshold, linearity, and resolution). The most important results obtained in this development are presented here.

2. Description of CrystalEyeCam Design and Components

In CrystalEyeCam, a high-density crystal scintillator is used to convert the X-ray image into visible light. A set of two turning mirrors and an objective relay the (visible) image from the scintillator to a highly sensitive, low-noise 16-bit CCD camera (see sketch in Figure 1 and photograph in Figure 2). The CCD camera (ROPER SCIENTIFIC, model LN/CCD-2048SB/2) is thinned, back-illuminated, and liquid nitrogen cooled. The CCD plane, 49 mm × 49 mm in dimensions, is made of 2048 × 2048, 24-μm square pixels.

The objective was specifically designed to match our needs. It has few chromatic and geometric aberrations and high photometric performances (high optical transmittance, no vignetting, and low f-number). It was produced by LINOS (model XCRL 162) and its main characteristics are listed below.

(i) Object working distance: 840 mm.

(ii) Object diameter: 270 mm.

(iii) Magnification: −0.258.

(iv) Effective f-number: 1.79 (at image plane).

(v) Distortion: less than 0.1%.

(vi) Through focus MTF: 86% for 4 lp/mm (at object plane).

(vii) Transmittance at 490 nm in wavelength: 86%.

(viii) Objective length and diameter: 392 mm & 190 mm.

(ix) Number of lenses: 7.

The two turning mirrors are intended to offset both the CCD camera and the objective lenses off the direct X-ray beam. This is necessary to protect the electronics and also because the lenses could emit light if the X-ray spectrum has a significant high-energy component (Cerenkov-light has an energy threshold of about 300 keV for regular glass [3]).

The scintillator cover is made of 7 mm of Aluminum alloy (AS7G) and 1.2 mm of Ta (intended for electronic equilibrium and filtering of low-energy scattered X-rays). The overall system is built with robustness in mind, so that it can sustain the harsh environment of shock physics experiments.

3. Moving from (Expensive) Segmented Scintillators to Monolithic Scintillator Assemblies

The level of noise in the image (thus, the signal-to-noise ratio) is directly linked to several of the scintillator characteristics as follows:

(i) density,

(ii) thickness,

(iii) mass attenuation coefficients (μ/ρ) (at the energies of the considered X-ray source),

(iv) the number of light photons emitted per unit of deposited dose,

(v) and optical transmittance at the wavelengths of the emitted light.

In particular, good signal to noise ratio in the image requires a thick enough scintillator (i.e., high enough the stopping power), most often at the expense of system

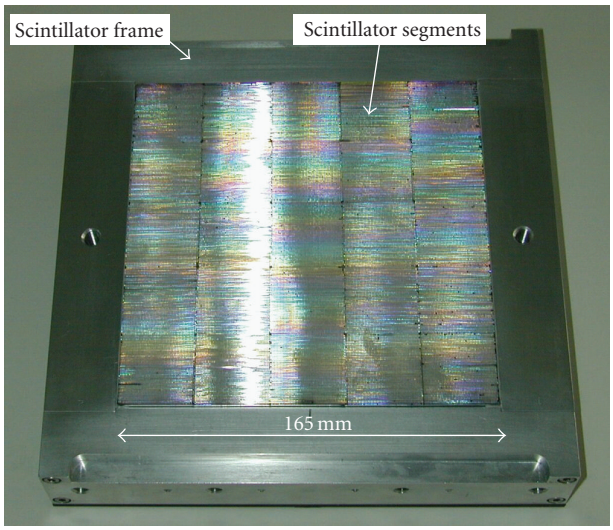

Figure 3: Photograph of the segmented scintillator (165 mm × 165 mm). It is assembled from 600 μm × 600 μm × 40 mm segments. The BGO crystal segments are each optically polished on all 6 sides. They are bonded together along with aluminized Mylar to make each segment optically independent and to reinforce the optical guiding properties of the segments.

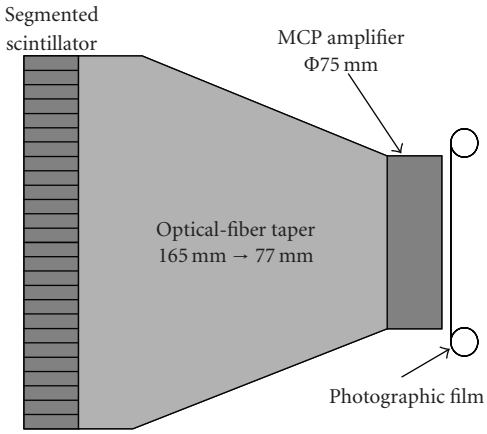

Figure 4: Sketch of the film radiographic camera previously used on AIRIX; the segmented BGO scintillator (165 mm × 165 mm) was optically coupled to a photographic film through a fiber taper and a Microchannel-Plate (MCP) amplifier.

resolution. To overcome that limitation, segmented scintillators were developed to produce both high stopping power and high-resolution imagers.

In the past, we fielded a segmented scintillator made of 600 μm × 600 μm segments (see Figure 3). The dimensions of this scintillator are 165 mm × 165 mm × 40 mm. The segments are made of Bismuth Germanate $Bi_4Ge_3O_{12}$ (BGO) crystal. It was originally coupled to photographic films through a fiber optic taper and a Microchannel-Plate (MCP) [1] for use on AIRIX (see diagram in Figure 4). In the imager, the scintillator is optically coupled to the film with a very high angular aperture. Consequently, if we were to use monolithic

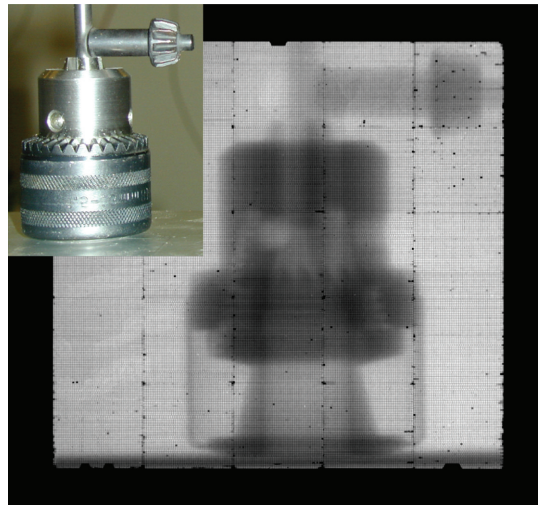

Figure 5: Radiograph of the test object (a driller chuck) using the segmented BGO scintillator and an unfiltered 18-MeV-bremsstrahlung spectrum. Note the few broken segments (black spots in the image) and the dead areas at some of the glue joints.

scintillator instead of segmented scintillators in this imager, we would be limited to thin scintillators only. Indeed, using scintillators thicker than several millimeters would result in very poor resolution (also several millimeters). So unless the available dose is very high or one can integrate the (low) dose for a long time, one has to rely on segmented scintillators in such imagers for multi-MeV radiography.

This segmented scintillator was also coupled to CrystalEyeCam during preliminary testing. As an illustration, we show a radiograph of a test object (a driller chuck) in Figure 5. The radiograph was obtained at the ELSA facility [2] with an unfiltered 18-MeV-bremsstrahlung spectrum. As is visible in the image, aside from a few broken segments (the black regions in the image), some of the glue interfaces cause noticeable dead areas. The light yield also varies from one segment to another, and this must be accounted for in the image after processing. Whereas the segmentation technique provides high stopping power and high resolution, it unfortunately brings losses in the image quality through the dead zones/spots and the (nonuniform) segmentation of the image. Finally, one limitation is the available segment size (and, as a result, the maximum resolution); for such a large segmented scintillator, 500–600 μm in segment dimension is the lowest that can practically be manufactured with BGO.

In radiographic cameras such as the CrystalEyeCam camera, it is possible to use thick monolithic scintillators (up to a few centimeters) in place of a segmented scintillator and still get good resolution [4, 5]. This is illustrated in Figure 6. When a monolithic scintillator is coupled to a CCD-based optical system through reasonably small angular aperture (parameter (α) in the figure), the voxel (elementary volume in the scintillator viewed by a CCD pixel) remains small enough. Its size depends specifically on the refractive index (n) of the scintillator, the angular aperture (α) of the objective at the object plane, and the size of the CCD

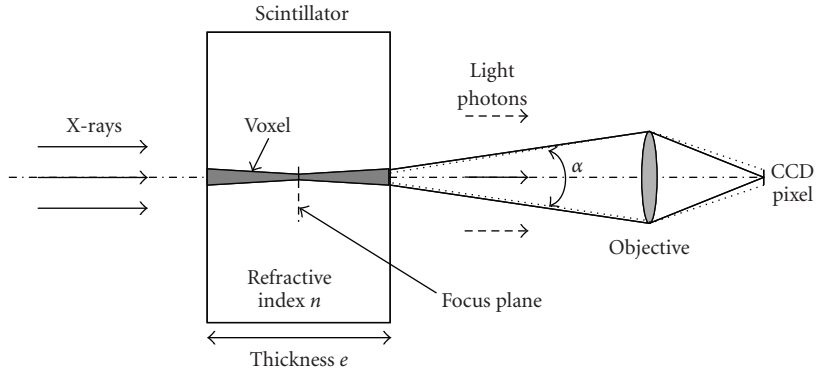

Figure 6: Schematic representation of the optical coupling of a CCD camera to a monolithic scintillator. The voxel (gray in the sketch) is the elementary volume viewed in the scintillator by a CCD pixel. Its size specifically depends on the refractive index (n) of the scintillator, the angular aperture (α) of the objective (at the object plan), and the size of the CCD pixel.

pixel. What we call "reasonably" small angular aperture is typically 10 degrees or less and is actually a common configuration. Indeed, standard commercial objectives are generally less than 80 mm in diameter so, when this objective is located further than 450 mm from the scintillator, the induced angular aperture (at the object plane) is less than 10 degrees in angle. However, it is best not to set too long a distance from the scintillator for the benefit of the system sensitivity; the closer, the better the photometric coupling. In the CrystalEyeCam camera, the angular aperture, at the object plane, is about 8 degrees in angle.

Industrial manufacturing techniques of the best suited crystals for multi-MeV X-ray imaging (i.e., those having both high-density and good-light yield, and which can be manufactured with very few or no visible defects in the bulk) do not currently allow production of blocks as large as 300–400 mm. Manufacturers are only able to produce blocks of high-quality BGO with uniform light yield and with no major defects (such as microscopic cracks or small bubbles) up to approximately 80 mm × 250 mm (with a maximum thickness of about 35 mm). In case of Cesium-doped Lutetium Yttrium Orthosilicate $Lu_{2(1-x)}Y_{2x}SiO_5 : Ce$ (LYSO), the maximum size is even smaller (approximately 70 mm × 100 mm at the present time, in thicknesses less than 30 mm). These limitations are mainly due to the fabrication process; such crystals are grown at high temperature (the value of which depends on the crystal). The size limitation is directly linked to the induced temperature gradients in the crystal. Cesium Iodide (CsI) and Sodium Iodide (NaI) crystals can be manufactured in larger sizes (typically up to 200 mm × 200 mm and 400 mm × 400 mm, resp.); however, these crystals have lower density and are rather hygroscopic. In addition, according to our supplier, the number of defects present in these crystals is noticeably higher (particularly with CsI) which makes them poorer candidates than BGO or LYSO for our imaging applications. For instance, in [4], the author reports about 20 to 30 flaws, 0.1 to 4 mm in width, randomly spread over the volume of their 12-mm thick, 230 mm × 230 mm in dimension, CsI(Tl) crystal. Such defects, which scatter the light produced within the scintillator, produce visible specks in the final image. We usually check the quality of our crystals using UV lamps and, to this day, none of the BGO or LYSO blocks we have purchased has presented any visible defects.

To overcome the size limitation of these crystals, we decided to develop specific assembling techniques for monolithic subelements; the challenge was to make the joints between crystals have minimum effect on the resulting images. In our early attempts, we tried producing assemblies by coupling crystals with optical glue (the crystal sides having been optically polished). Optical glues have refractive indexes up to 1.7, and high-density crystals such as BGO and LYSO have refractive indexes close to 2. So, even though no optical glue could match the high-refractive index of these crystals, we hoped that the light diffusion at the joint would be kept at reasonably low level. Unfortunately, it does not appear to be so, as illustrated in Figure 7. This image was obtained with a scintillator assembly made of four 55 mm × 55 mm LYSO blocks, 10 mm in thickness, and an unfiltered 18-MeV-bremsstrahlung spectrum. The speckles on the image are due to scattered (ionizing) radiation interacting directly with the CCD potential wells. These speckles could easily be treated using median filter, but we left them on this image as an illustration (all the other images presented thereafter were properly treated to produce speckle-free images). The image shows that the joints between blocks (as well as the edges) are very bright; the residual microchamfers on the edges of the glued sides diffuse significant level of light in the direction of the objective. Moreover, two types of backing were used in this experiment: black cardboard on the upper left in the image and white glossy paper on the lower right. The diffusion (at the joints and on the edges) is both amplified and spread when white paper is used; the amplification is due to the reflective properties of the backing which induce losses in the system resolution. With segmented scintillators, reflective backing (aluminized Mylar, white paint, etc.) is frequently used to increase the sensitivity of the imager (especially because it has no impact on the resolution). With a (thick) monolithic scintillator to keep resolution optimum (for a given scintillator thickness) and to avoid amplifying

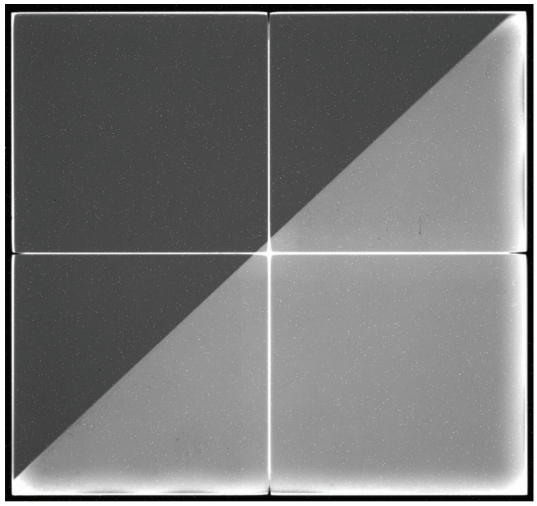

Figure 7: Radiograph obtained using a 10 mm thick, 110 mm× 110 mm scintillator assembly and an unfiltered 18-MeV-bremsstrahlung spectrum. The scintillator is made of four 55 mm × 55 mm LYSO scintillators, assembled using optical glue. Two types of backing (placed on the X-ray side of the scintillator) were used in this experiment; black cardboard on the upper left of the image and white glossy paper on the lower right. The glue joints appear brighter than the bulk of the scintillator.

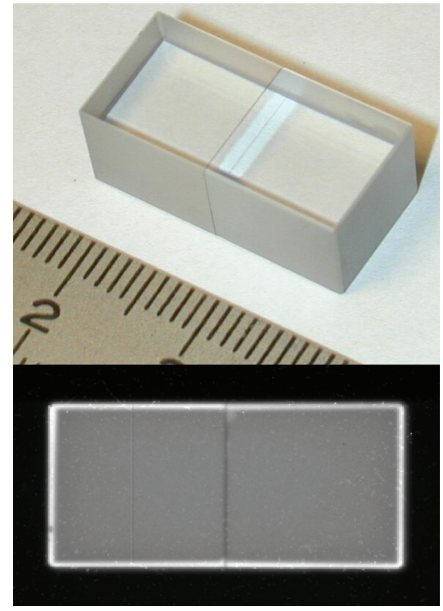

Figure 8: Radiograph obtained with a small BGO sample made of two 10 × 10 × 10 mm cubes glued together with absorptive glue; the joint appears darker than the bulk of the scintillator which is a desirable condition.

the joint perturbation, it is necessary to use an absorbing material, such as black cardboard or black paint, on the side of the scintillator that faces the X-ray source.

After several trials and developments, we eventually validated a design where the joint optical effect is minimized. This design, which uses a nontransparent glue, is fully detailed in [6] and leads to relatively small apparent joint thicknesses (typically about 200 μm on large-dimension assemblies). Since our objective (de-)magnification is about 1 : 4, and our CCD plane is made of 24-μm pixels, a 200-μm thick joint should theoretically only impact about 2 pixels on the CCD. However, due to the actual resolution of the entire system and because of parallax effects (especially with such a large diameter objective), the effect of the joint spreads over a few more pixels depending on the scintillator thickness. For example, we initially tested the design on a small sample, made of two $10 \times 10 \times 10$ mm BGO cubes glued together, and obtained satisfying results (see Figure 8, the radiograph was obtained with unfiltered 18-MeV-bremsstrahlung spectrum); the joint does not diffuse excessively (it appears darker than the bulk of the scintillator) and spreads over about 4 pixels.

As an illustration of what image quality can be obtained with larger dimension assemblies, we produced a radiograph of the driller chuck using a 20 mm thick, 165 mm × 165 mm BGO assembly made of two blocks (see photograph in Figure 9, this assembly has been manufactured by Saint-Gobain Cristaux et Détecteurs [6]). The resulting radiograph is shown in Figure 10; we used 18-MeV-bremsstrahlung spectrum, filtered with 10 cm of lead. The lead filter is intended to reproduce the typical spectrum reaching our imagers in actual shock physics experiments. The resolution

Figure 9: Photograph of a prototype of monolithic BGO assembly; it is made of two 20-mm-thick blocks and is 165 mm × 165 mm in size.

of our imager with this source is about 1 mm, and the image quality is highly improved when compared to that obtained in Figure 5 with the segmented scintillator.

Note that, as illustrated in Figure 6, to optimize the system resolution, the objective needs to focus inside the (monolithic) scintillator. The optimal location of the focus plane depends on many parameters: the refractive index of the scintillator, the angular aperture of the objective at

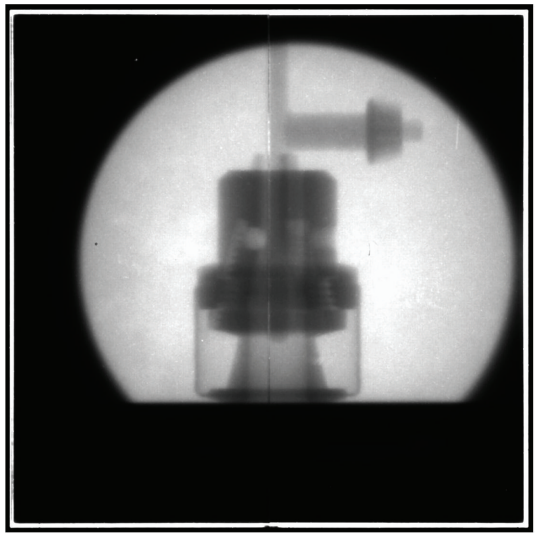

Figure 10: Radiograph of a driller chuck using the prototype monolithic BGO assembly and an 18-MeV-bremsstrahlung spectrum, filtered with 10 cm of lead. The joint, which remains slightly apparent on this image, could easily be removed using field-flattening techniques. The X-ray beam was collimated to limit the level of scatter radiation interacting with the CCD.

the object plane, the size of the CCD pixel, the magnification and the resolution of the objective, the energy spread in the scintillator (for the specific X-ray spectrum of the source), and so forth. For BGO and LYSO assemblies, with thicknesses in the 10 to 40 mm range (and filtered 18-MeV-bremsstrahlung spectrum), our measurements have shown that a good approximation of the optimal coupling configuration is to focus in the middle of the scintillating material as represented in Figure 6 (for instance, in a 40-mm-thick scintillator, the optimal focus plane is actually about 15-16 mm from the side facing the X-ray source).

In addition to reaching better quality images with these crystal assemblies, the cost of manufacturing is also lower by an order of magnitude; the production of the segmented scintillator shown in Figure 3 requires polishing and gluing the 6 faces of each of the 62500 BGO segments.

4. System Performance as a Function of Scintillator Thickness

Often, the radiographic test objects are thick and dense enough, so that the imagers operate at a level close to their detection threshold. Before performing the (irreversible) actual experiment, it is crucial to make sure that the data will be good enough to produce the measurements of interest. This implies developing and using simulation codes that can produce accurate predictions of the expected experimental images. Thus, it is necessary to precisely measure and model the imager performances in these codes.

Measurements of CrystalEyeCam noise, sensitivity, detection threshold, and resolution were performed using two BGO assemblies (in different thicknesses); the results are presented in the following sections.

4.1. Noise Measurements. The noise was studied in two steps. We first performed a characterization of the CCD camera itself (along with the objective and mirrors), using a light source in place of the scintillator. We used the Lumitex fiber optic light panel that is integrated inside the scintillator cover to provide test points of the system whenever needed (see Figure 11). A set of diffusers were placed in front of the light source to produce uniform illumination of the CCD. Measurements were performed at various light levels in order to cover most of the CCD operating range. Figure 12 provides a plot of the standard deviation of the noise (σ) as a function of the signal level (S) in the image (i.e., the mean value in the image above offset). The standard deviation of the noise was estimated after the fixed pattern (systematic) noise was removed from the image. This can either be done by subtracting two flat-field images of the same level (and accounting for the induced increase in noise through this subtraction) or using specific image processing techniques on single images. In our case, we chose the latter option; we processed the numerical Laplacian of the image and fit a Gaussian function on its histogram [7].

The resulting curve is usually called the CCD Photon Transfer Curve (PTC). We modeled it with the function described below

$$\sigma^2 = \sigma_0^2 + k \cdot S, \tag{1}$$

where $\sigma_0 = 5.1$ LSB. (Least Significant Byte) and $k = 0.81$ LSB.

In this expression, the first term accounts for the read noise-limited regime, and the second one models the quantum noise-limited regime (with its standard curve slope of 1/2 on a log-log graph). $1/k$ (=1.23 electrons/LSB) is the CCD gain and σ_0 is the read noise level (5.1 LSB, i.e., ~6 electrons).

In a second step, we studied the full system using X-rays and two different scintillator assemblies successively (including the one shown in Figure 9). They were both 165 mm × 165 mm and constructed with two BGO blocks, the only difference being their thickness: 20 and 30 mm, respectively. The interaction probability of an X-ray with our BGO assemblies depends on the photon energy and on the scintillator thickness; for 4-MeV X-rays, it is estimated to be 45% and 57%, respectively. The theoretical (energy) stopping power of the 20-mm thick BGO assembly is 30% for 4-MeV X-rays, and it reaches 41% with the 30-mm thick BGO assembly.

The radiographic data provided here were obtained using a filtered 18-MeV-bremsstrahlung spectrum. Various doses were applied in order to cover the lower range of detection of the camera, where most of our experiments take place. The noise and signal levels were obtained using the same image processing as described above. The results are shown in Figure 12, where it is clear that they overlay nicely with those obtained from the light source. This indicates that the noise of the system is dominated by the (dark and quantum)

Table 1: CrystalEyeCam sensitivities, detection thresholds and resolutions obtained with two scintillator thicknesses, and an 18-MeV-bremsstrahlung spectrum, filtered with 10 cm of lead.

BGO scintillator thickness	System sensitivity in LSB/μGy(air)	System detection threshold (at $SNR_0 = 2$) in μGy(air)	System resolution-FWHM(LSF) in mm	System cutoff frequency (MTF at 0.5) in mm^{-1}
20 mm	7.6	1.6	0.83	0.174
30 mm	11.5	1	0.98	0.166

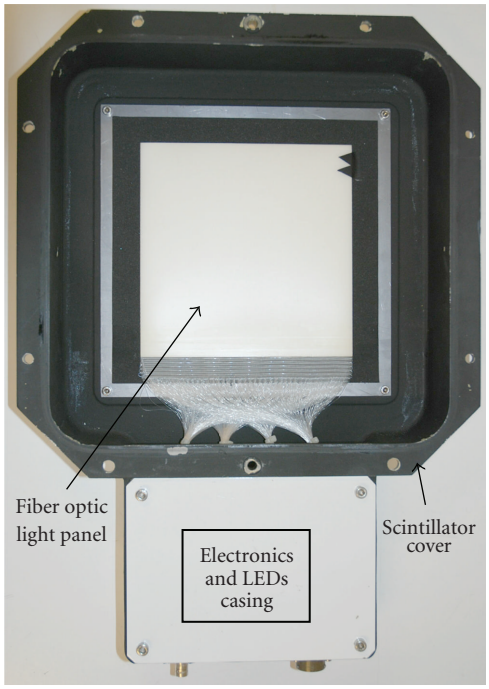

Figure 11: Photograph of the inside of the scintillator cover; the bottom of the cover includes electronics to power Light-Emitting Diodes (LEDs). The emitted light is guided from the LEDs to a Lumitex fiber optic light panel through optical fibers. The light panel is used to shine the scintillator and provide test points of the system whenever needed.

noise produced in the CCD, and the imaging system acts as a quantum sink. Performing the optical coupling of the scintillator to the CCD with an objective (i.e., through a rather small angular aperture) permits the use of monolithic scintillators and produces better quality imaging than with segmented scintillators, but there is a drawback; the X-ray quantum noise is not the dominant source of noise in our system. According to our estimate, one 4-MeV X-ray photon interacting with a 30-mm-thick BGO scintillator produces less than 5 visible photons detected by the CCD. Fortunately, CCD manufacturers are able to produce high-sensitivity, low-noise cameras, and our system performance remains quite good. When Monte Carlo codes are used to simulate the radiographic image (see [8–10]), (1) is helpful to calculate the additional contribution of the imager to the noise in the final image.

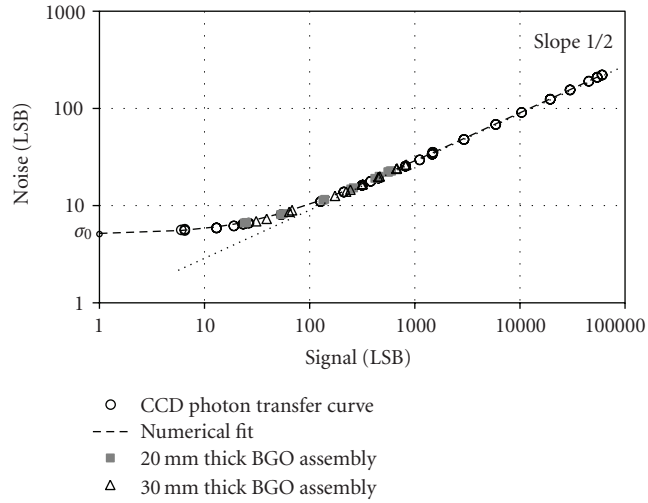

Figure 12: Photon transfer curve (open circles) of the CCD; noise (σ) produced in the CCD as a function of signal level (S) (measurement performed with a light source); (dashed line) numerical fit of the experimental curve ($\sigma^2 = \sigma_0^2 + k \cdot S$, with $\sigma_0 = 5.1$ LSB and $k = 0.81$); noise produced in the imager as a function of signal level with 20-mm (solid grey squares) and 30-mm (open triangles) thick BGO scintillators, respectively (measurement performed using X-rays). Note that all measurements overlay nicely, indicating that the dominating contributor to the imager noise is the noise produced in the CCD.

4.2. Detection Threshold. Equation (1) can be used to calculate the detection threshold (T) of the imager for a given signal-to-noise ratio (SNR_0). In our applications, we usually calculate the detection threshold for a signal-to-noise ratio $(SNR_0) = 2$.

(T) is the solution to the equation $SNR_0^2 = (S/\sigma)^2$, where (S) is the unknown.

In other words, $SNR_0^2 = T^2/(\sigma_0^2 + k \times T)$ and one can show that $T = 2k + 2\sqrt{k^2 + \sigma_0^2} \approx 12$ LSB.

With the sensitivity of the (linear) imaging system (A) expressed in LSB/μGy(air) (and depending on the scintillator thickness), the detection threshold for $SNR_0 = 2$ can be expressed as

$$T\ (\mu\text{Gy(air)}) \approx \frac{12}{A(\text{LSB}/\mu\text{Gy(air)})} \quad (\text{at } SNR_0 = 2). \quad (2)$$

Values of our system sensitivity (along with the associated thresholds) for both scintillator assemblies are reported in Table 1. The doses used to calculate the sensitivities

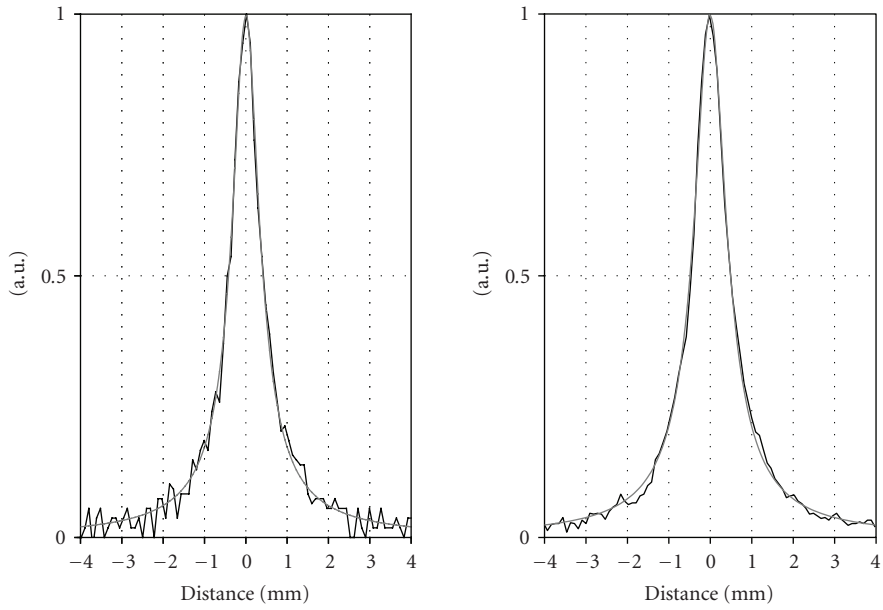

Figure 13: Resolution measurements of the imager for various scintillator thicknesses, using the regular roll bar method and an 18-MeV-bremsstrahlung spectrum, filtered with 10 cm of lead; the experimental images were analyzed to infer the line spread functions (LSFs) shown. Results for the 20-mm thick BGO assembly are shown on the left and results for the 30-mm thick BGO assembly are shown on the right: experimental results (thin black lines) and plots of the associated fit functions (thick gray lines).

were measured with about 15% uncertainty in these experiments.

4.3. Resolution Measurements. Resolution measurements were also performed using the regular roll bar method (see [11]). The images were analyzed to infer the Line Spread Functions (LSFs), which were numerically fit using the function expressed below

$$f(x) = \frac{a_1}{\left[1 + \left((x - a_2)/a_3\right)^2\right]^{a_4}}, \tag{3}$$

where a_1, a_2, a_3, and a_4 are the free parameters of the fit.

This function is convenient because it includes both the Lorentz ($a_4 = 1$) and Bennett ($a_4 = 1.5$) functions that are commonly used to fit LSFs (or MTFs) in radiographic analysis.

The resulting LSFs are plotted in Figure 13, along with their fit functions. Prior to the fits, we normalized the data to the origin and divided the LSFs by their values at the origin. As a result, parameter a_1 equals 1 and parameter a_2 equals zero. The obtained (a_3, a_4) parameters were (0.356, 0.803) and (0.433, 0.840) for the 20-mm-thick and 30-mm-thick assemblies, respectively. A Fourier transform was applied to the fit functions of the Line Spread Functions in order to produce the Modulation Transfer Functions (MTFs) (see Figure 14). The Full Widths at Half Maximum (FWHM) of the LSFs and the cutoff frequencies at 50% of the MTF maximums are provided in Table 1.

As a comparison, the detection threshold and the resolution of the film radiographic camera previously in use at AIRIX [1] (using the segmented scintillator shown in Figure 3) were ~0.1 μGy(air) and ~1.5 mm, respectively. Also, when this same segmented scintillator is coupled to CrystalEyeCam, the detection threshold and resolution are ~1 μGy(air) and ~1.2 mm, respectively. In both cases, a reflective backing (aluminized Mylar) was placed on the

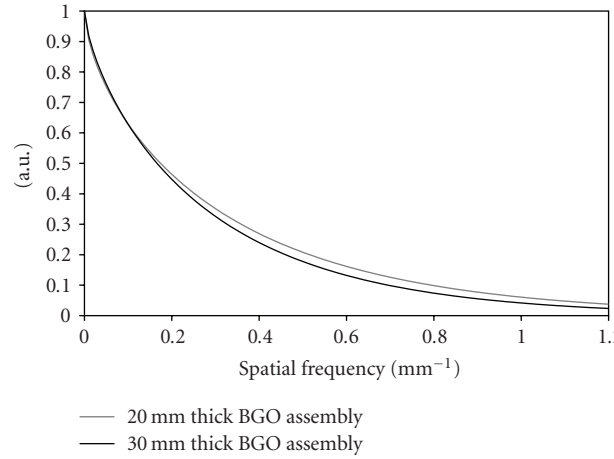

Figure 14: The modulation transfer functions (MTFs) of the imager, as a function of scintillator thickness, were obtained by applying a Fourier transform to the fit functions of the experimental line spread functions. MTF obtained with the 20-mm thick BGO assembly (gray line); MTF obtained with the 30-mm thick BGO assembly (black line).

segmented scintillator (on the X-ray side) to increase the light-coupling efficiency.

Although this system provides a better quality image (higher resolution and no segmentation), it is slightly less sensitive. However, the detection threshold could be improved by using LYSO instead of BGO (LYSO light yield is about 3 times higher than that of BGO). Since LYSO cannot be produced in pieces as large as for BGO for a given size of scintillator assembly, more glue joints would be required and be present in the image.

5. Conclusion

We have fielded a new CCD-based radiographic camera, called CrystalEyeCam, at the AIRIX facility for use in shock physics experiments. CrystalEyeCam is composed of two turning mirrors and an objective to relay the (visible) image from a scintillator assembly to a highly sensitive, low-noise CCD camera. The objective was specifically developed to match our needs and has few chromatic and geometric aberrations and high photometric performance. The scintillator assembly is constructed using a specific (patented) technique of assembling monolithic scintillating crystals. It replaces the segmented scintillator previously used at the facility and produces higher quality images (better resolution and no segmentation). The performance of CrystalEyeCam was measured using an 18-MeV-bremsstrahlung spectrum, filtered with 10 cm of lead, and two 165 mm × 165 mm BGO assemblies: 20 and 30 mm in thickness, respectively. With the 30-mm-thick BGO assembly, the measured detection threshold of the imager (at $SNR_0 = 2$) is 1 μGy(air) and its resolution is ∼1 mm. For 4-MeV incident photons, the estimated stopping power of the scintillator is 41%. The scintillator assembly thus proved to be a cheaper, effective alternative to segmented scintillators for use in CrystalEyeCam.

The next generation of imager, CrystalEyeCam II, is already in construction. It will include a larger radiographic field of view (190 mm × 190 mm), an improved mechanical design (better shielding to scatter X-rays) and a more recent CCD camera with convenient thermoelectrical cooling (instead of liquid nitrogen). The use of LYSO assemblies is also considered to improve the detection threshold.

Acknowledgments

The authors would like to thank P. Balleyguier, A. Binet, A. Bloquet, J.-L. Flamand, V. le Flanchec, V. Jacob, M. Millérioux, and G. Vallard for their help in setting up and performing the experiments at ELSA facility. C. Aedy and S. Quillin are thanked for our many interesting discussions on high-energy flash X-ray imaging. They are indebted to D. B. Holtkamp for the numerous and helpful discussions on shock physics experiments. They also wish to thank B. Angelier, J. Bénier, N. Brousse, S. Darbon, and P. Millier, who contributed to the initial design and development of CrystalEyeCam. The authors are also indebted to the referee for very interesting remarks.

References

[1] E. Merle, J. Delvaux, M. Mouillet, O. Pierret, D. Noré, and C. Vermare, "The firsts years with the AIRIX flash X-ray radiographic facility," in *25th International Congress on High-Speed Photography and Photonics*, Proceedings of SPIE, pp. 652–657, Beaune, France, October 2003.

[2] P. Guimbal, P. Balleyguier, A. Binet et al., "Status of the ELSA-2 project," in *Proceedings of EPAC*, p. 1768, Paris, France, 2002.

[3] M. F. L'Annunziata, "Cerenkov Counting," in *Handbook of Radioactivity Analysis*, p. 768, Elsevier Science, Amsterdam, The Netherlands; Academic Press, New York, NY, USA, 2003.

[4] A. Sawant, H. Zeman, S. Samant, G. Lovhoiden, B. Weinberg, and F. DiBianca, "Theoretical analysis and experimental evaluation of a CsI(Tl) based electronic portal imaging system," *Medical Physics*, vol. 29, no. 6, pp. 1042–1053, 2002.

[5] S. S. Samant, A. Gopal, and D. Sobczak, "A high quantum efficiency prototype video based portal imaging system," *Journal of X-Ray Science and Technology*, vol. 14, no. 3, pp. 161–175, 2006.

[6] D. Partouche-Sebban and I. Abraham, "Scintillateur pour dispositif d'imagerie, module scintillateur, dispositif d'imagerie avec un tel scintillateur et procédé de fabrication d'un scintillateur," French patent #2922319, 17 avril 2009, Present licensee: Saint-Gobain Cristaux et détecteurs, http://www.detectors.saint-gobain.com/.

[7] J.-M. Lagrange, *Reconstruction tomographique à partir d'un petit nombre de vues*, Ph.D. dissertation, École Normale Supérieure de Cachan, Cachan, France, 1998.

[8] E. C. Snow and J. D. Court, "Radiography. Image detector capability in MCNP4B," *Transactions of the American Nuclear Society*, vol. 79, p. 99, 1998.

[9] M. S. McKinley and A. E. S. von Wittenau, "Radiographic capabilities of the MERCURY Monte Carlo code," *Nuclear Technology*, vol. 168, no. 1, pp. 245–248, 2009.

[10] D. Riz, "Calculation and use of multigroup cross sections including electron-photon cascade for a 3D Monte Carlo neutron-gamma transport code. Comparisons with MCNP-4B," in *Proceedings of ANS PHYSOR*, American Nuclear Society, 2000, CD-ROM.

[11] E. Rose, R. Carlson, and J. Smith, "Radiographic performance of Cygnus 1 and the Febetron 705," in *Proceedings of the 14th IEEE International Pulsed Power Conference*, pp. 756–759, Dallas, Tex, USA, June 2003.